

Contents lists available at ScienceDirect

Petroleum Science

journal homepage: www.keaipublishing.com/en/journals/petroleum-science



Original Paper

Self-supervised simultaneous deblending and interpolation of incomplete blended data using a multistep blind-trace U-Net



Ben-Feng Wang *, Shi-Cong Lin, Xin-Yi Chen

State Key Laboratory of Marine Geology, Tongji University, Shanghai, 200092, China

ARTICLE INFO

Article history: Received 4 July 2024 Received in revised form 26 September 2024 Accepted 23 December 2024 Available online 25 December 2024

Edited by Meng-Jiao Zhou and Min Li

Keywords:
Blind-trace U-Net
Self-supervised learning
Simultaneous deblending and interpolation
Multi-step processing

ABSTRACT

Blended acquisition offers efficiency improvements over conventional seismic data acquisition, at the cost of introducing blending noise effects, Besides, seismic data often suffers from irregularly missing shots caused by artificial or natural effects during blended acquisition. Therefore, blending noise attenuation and missing shots reconstruction are essential for providing high-quality seismic data for further seismic processing and interpretation. The iterative shrinkage thresholding algorithm can help obtain deblended data based on sparsity assumptions of complete unblended data, and it characterizes seismic data linearly. Supervised learning algorithms can effectively capture the nonlinear relationship between incomplete pseudo-deblended data and complete unblended data. However, the dependence on complete unblended labels limits their practicality in field applications. Consequently, a selfsupervised algorithm is presented for simultaneous deblending and interpolation of incomplete blended data, which minimizes the difference between simulated and observed incomplete pseudodeblended data. The used blind-trace U-Net (BTU-Net) prevents identity mapping during complete unblended data estimation. Furthermore, a multistep process with blending noise simulationsubtraction and missing traces reconstruction-insertion is used in each step to improve the deblending and interpolation performance. Experiments with synthetic and field incomplete blended data demonstrate the effectiveness of the multistep self-supervised BTU-Net algorithm.

© 2025 The Authors. Publishing services by Elsevier B.V. on behalf of KeAi Communications Co. Ltd. This is an open access article under the CC BY-NC-ND license (http://creativecommons.org/licenses/by-nc-nd/

4.0/).

1. Introduction

Blended acquisition fires multiple sources with overlapping firing time, enhancing efficiency compared to conventional acquisition (Beasley et al., 1998; Berkhout, 2008). Besides, irregularly missing shots in certain acquisition cases result in blended data with missing information, which is referred to incomplete blended data. Blending noise and missing traces pose great challenges for subsequent seismic inversion and migration. Consequently, the process of deblending and interpolation is necessary to provide high-quality complete unblended data for seismic procedures.

Seismic deblending can be categorized into two types: filtering based and inversion based algorithms. Filtering based methods use different denoising algorithms to attenuate the blending noise. The blending noise often appears as spatially randomized and spike-like noise compared to coherent signals in common offset,

midpoint, receiver domains (Mahdad et al., 2011). Most filtering based methods use a median filter (MF) or its improved variations, such as multidirectional vector variation (Huo et al., 2012), spacevarying variation (Chen, 2015), structure-oriented variation (Gan et al., 2016b), and the combination of structure-oriented and space-varying MF (Chen et al., 2020). Although filtering based methods are efficient, the deblending performance remains open to improvement. Inversion based deblending methods achieve more accurate results (Abma et al., 2010) by solving an ill-posed problem with specific constraints such as the low-rank constraint (Cheng and Sacchi, 2015) and the sparsity constraint. The sparsity constraint is always employed via different sparse transforms, such as the Fourier transform (Abma et al., 2015), the Radon transform (Akerberg et al., 2008; Ibrahim and Sacchi, 2013), the curvelet transform (Zu et al., 2016) and the seislet transform (Chen et al., 2014; Gan et al., 2016a). For incomplete deblended data, Zhou and Li (2018) simultaneously attenuated spike-like blending noise and reconstructed missing traces by applying iterative structureoriented median and mean filtering. The curvelet (Zu et al., 2016)

E-mail address: wbf1232007@tongji.edu.cn (B.-F. Wang).

^{*} Corresponding author.

and the double focal (Cao et al., 2019) transforms were also explored for joint deblending and interpolation. Wang et al. (2022a) implemented iterative thresholding based on the sparse Fourier and curvelet transforms for simultaneous deblending and interpolation in 3D cases. However, hyperparameter selection in traditional methods typically requires greater expertise or experience, which limits flexibility and makes it more challenging to achieve optimal parameter settings. Additionally, traditional methods tend to struggle with the efficient processing of large-scale blended data. The large data volume poses significant computational challenges, leading to slower processing speeds and increased computational costs. Despite the wide applications, its accuracy still leaves opportunities for enhancement.

Other than traditional deblending and interpolation methods, deep learning based deblending methods can nonlinearly map the input to the desired output (Sun et al., 2019; Zu et al., 2020). Once well-trained or fine-tuned, the optimized model can be applied to test data that have similar characteristics as the training data (Richardson, 2019; Wang et al., 2021). Zu et al. (2022) introduced a supervised deblending model based on a Transformer to extract vertical, horizontal, and local features. Sun et al. (2022) constructed the training dataset based on practical acquisition situations to decrease the cost of simulating training datasets. To further reduce the dependence on unblended labels, unsupervised and selfsupervised deblending strategies are employed. Deep Image Prior (DIP) was introduced to avoid the need for constructing a huge training dataset and to achieve adaptive deblending performance at the cost of sizeable computational time and resources (Xu et al., 2021). Xue et al. (2022) designed a loss function to measure the difference between the observed pseudo-deblended data and the corresponding simulated result using the estimated signal. Wang et al. (2023a) combined the Res-Net and U-Net to construct a unified loss function for unsupervised deblending. After pseudodeblending, common receiver gathers (CRGs) and common shot gathers (CSGs) are of significant coherence similarities. It is feasible to utilize the pseudo-deblended CSG and its blending-pseudodeblending result as a training pair for DNNs, with subsequent deblending for the pseudo-deblended CRGs (Wang and Hu, 2022; Xu et al., 2022). Based on the supervised multistep approach (Wang et al., 2023) which can quantitatively evaluate the remaining blending noise, Chen and Wang (2024) designed a self-supervised multistep deblending method utilizing a CSG constructed adaptive training dataset. The key to the above self-supervised strategy lies in the construction of an adaptive training dataset, which assumes consistent spatial sampling in the training CSGs and the test CRGs. The assumption, however, is seldom available in field cases, especially when considering irregularity effects. The blind-trace network (Laine et al., 2019), which modifies the convolution and max-pooling operations, enables the applicability of selfsupervised seismic data processing. Treating pseudo-deblended seismic data as images, a self-supervised blind-trace U-Net (BTU-Net) deblending framework was designed (Wang et al., 2023b). Luiken et al. (2023) embedded a blind-trace denoiser in the plugand-play algorithm for deblending.

This paper suggests a multistep algorithm to attenuate blending noise and reconstruct missing shots in a self-supervised manner. We design a self-supervised loss function that operates without clean labels requirement, and a BTU-Net is adopted to prevent learning from identity. Numerical tests on synthetic artificially incomplete blended data indicate that our proposed algorithm outperforms the conventional curvelet based iterative shrinkage thresholding algorithm (ISTA). Field incomplete blended data example further shows its effectiveness in providing complete deblended data estimation for subsequent seismic processing.

2. Method

2.1. Incomplete blended acquisition

Blended acquisition has been widely used in field surveys as an alternative to conventional one to improve acquisition efficiency. Fig. 1 compares conventional seismic acquisition (Fig. 1(a)) and incomplete blended acquisition with irregularity considerations (Fig. 1(b)).

In conventional acquisition (Fig. 1(a)), shots are fired with sufficient firing time intervals to obtain unblended seismic record d without blending interference. The acquired data can assist seismic processing and migration algorithms to characterize subsurface structures. Blended acquisition fires multiple seismic sources in different regions almost simultaneously, significantly enhancing acquisition efficiency through overlapping firing times. Besides, the acquired blended data is sometimes contaminated by missing shots caused by various factors, like surface obstacles. Fig. 1(b) illustrates blended acquisition with a blending fold of 2 and irregularly missing shots considerations. For a given receiver r_i , i = 1, 2, ..., Nr among Nr receivers, the observed incomplete blended data is expressed in Eq. (1),

$$d_{\text{obs}}(t, r_i) = \sum_{j \in S} d(t + \tau_j, s_j, r_i), i = 1, 2, ..., Nr,$$
(1)

where, the symbol τ_j represents the dithering time of the available shot s_j , $j \in S$, as marked by the stars. The unavailable shots are marked by the crosses in Fig. 1(b). Eq. (1) can be reformulated in a matrix form,

$$\mathbf{d}_{obs} = \mathbf{\Gamma} \mathbf{R} \mathbf{d},\tag{2}$$

where \mathbf{d}_{obs} represents the recorded incomplete blended data, Γ represents the blending operator, and \mathbf{R} is a sampling operator determined by whether the shot is available or not during blended acquisition. The shooting time and location are known during blended acquisition, allowing the precise construction of the blending operator Γ and the sampling operator Γ . They can link incomplete blended data \mathbf{d}_{obs} with complete unblended data \mathbf{d} as shown in Eq. (2). The incomplete pseudo-deblended data \mathbf{d}_{pdb} is obtained using the adjoint blending operator Γ^H ,

$$\label{eq:dpdb} \boldsymbol{d}_{pdb} = \boldsymbol{\Gamma}^{H}\boldsymbol{d}_{obs} = \boldsymbol{R}\boldsymbol{d} + \left(\boldsymbol{\Gamma}^{H}\boldsymbol{\Gamma} - \boldsymbol{I}\right)\!\boldsymbol{R}\boldsymbol{d}, \tag{3}$$

where **Rd** represents incomplete unblended data and $(\Gamma^H\Gamma - I)$ **Rd** represents the blending noise. According to Eq. (3), the signal is affected by both blending noise and irregularities. For better illustrations, Fig. 2(a) presents a complete unblended CRG, while Fig. 2(b) shows the corresponding incomplete pseudo-deblended CRG with 50 percent irregularly missing traces and a blending fold of 3. Incomplete pseudo-deblended data poses challenges for subsequent seismic processing algorithms in accurately depicting

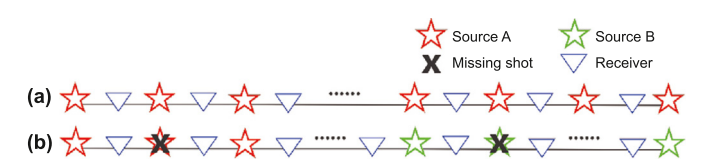


Fig. 1. Comparison of (a) conventional seismic acquisition and (b) incomplete blended acquisition with irregularity considerations.

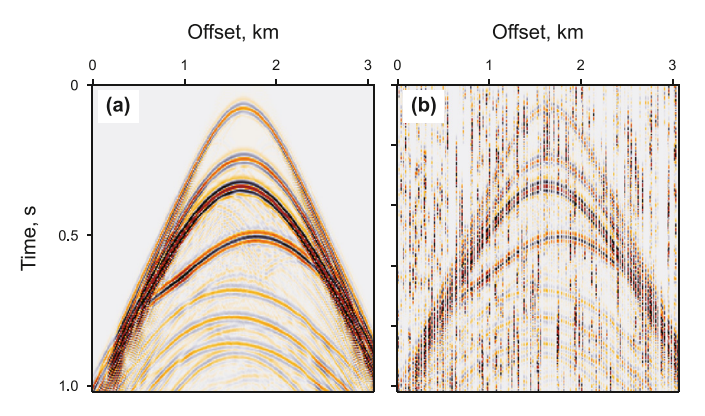


Fig. 2. (a) A complete unblended CRG; (b) the incomplete pseudo-deblended CRG.

subsurface structures. Consequently, it is essential to provide highquality data through blending noise attenuation and missing traces reconstruction.

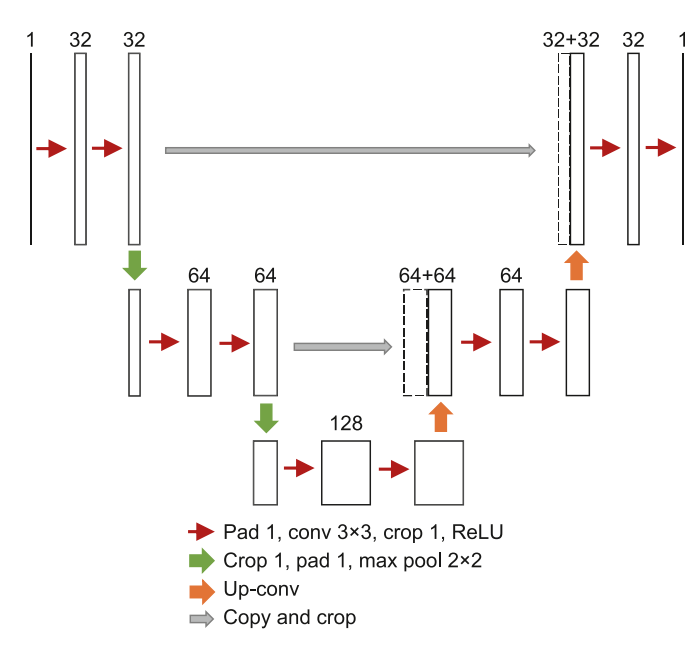


Fig. 3. The BTU-Net architecture for self-supervised simultaneous deblending and interpolation.

2.2. Simultaneous deblending and interpolation by sparsity-promotion

Blending noise can affect the reconstruction accuracy of incomplete data, while the missing traces also hinder the deblending performance of blended data (Wang et al., 2022a). Thus, simultaneous deblending and interpolation is beneficial for processing incomplete blended data.

Complete unblended data can be sparsely characterized through sparse transforms, and the sparsity promotion algorithm can be iteratively used for simultaneous deblending and interpolation based on compressive sensing. For incomplete blended data $\mathbf{d}_{obs} = \mathbf{\Gamma}\mathbf{R}\mathbf{d}$, the iterative estimation of complete unblended data can be shown as follows using the ISTA,

$$\mathbf{d}_{dbl}^{j+1} = \mathbf{C}^{H} T_{\lambda} \mathbf{C} \left(\mathbf{\Gamma}^{H} \mathbf{d}_{obs} - \left(\mathbf{\Gamma}^{H} \mathbf{\Gamma} - \mathbf{I} \right) \mathbf{R} \mathbf{d}_{dbl}^{j} + (\mathbf{I} - \mathbf{R}) \mathbf{d}_{dbl}^{j} \right),$$

$$j = 1, 2, \dots, J,$$

$$(4)$$

where \mathbf{d}_{dbl}^{j} is the jth iterative unknown estimation, with a defined maximum iteration number *J*. The operators \mathbf{C} and \mathbf{C}^{H} represent the forward and inverse curvelet transforms, respectively. The symbol T_1 represents a hard thresholding operator with the threshold λ selected via a cooling strategy by trial and error according to incomplete pseudo-deblended data. During deblending, the simulated blending noise $(\Gamma^H\Gamma-I)R\boldsymbol{d}_{dbl}^j$ is subtracted from $\Gamma^H\boldsymbol{d}_{obs}$, and the reconstructed traces $(\mathbf{I} - \mathbf{R})\mathbf{d}_{dbl}^{j}$ are inserted to update the input for further sparsity characterization. When the iteration number reaches the user defined maximum J, the recovery result can be obtained for subsequent seismic processing procedures. Even so, the accuracy of sparse transforms is limited because they linearly characterize seismic data. Conversely, deep learning strategies serve as a more effective tool for accurate nonlinear seismic data characterization, holding the potential to enhance recovery accuracy.

2.3. Self-supervised simultaneous deblending and interpolation

A supervised strategy can extract the nonlinear relationship between the incomplete pseudo-deblended data (\mathbf{d}_{pdb}) and the complete unblended one (\mathbf{d}), using labeled pairs. Once the network is well-trained with optimized parameters θ^* , it can be inferred for simultaneous deblending and interpolation of test data \mathbf{d}_{pdb_t} via $f(\mathbf{d}_{pdb_t}; \theta^*)$. However, one of the challenges is the large number of labels requirement to train the designed network, as complete unblended data is rarely accessible in field cases. Since the blending

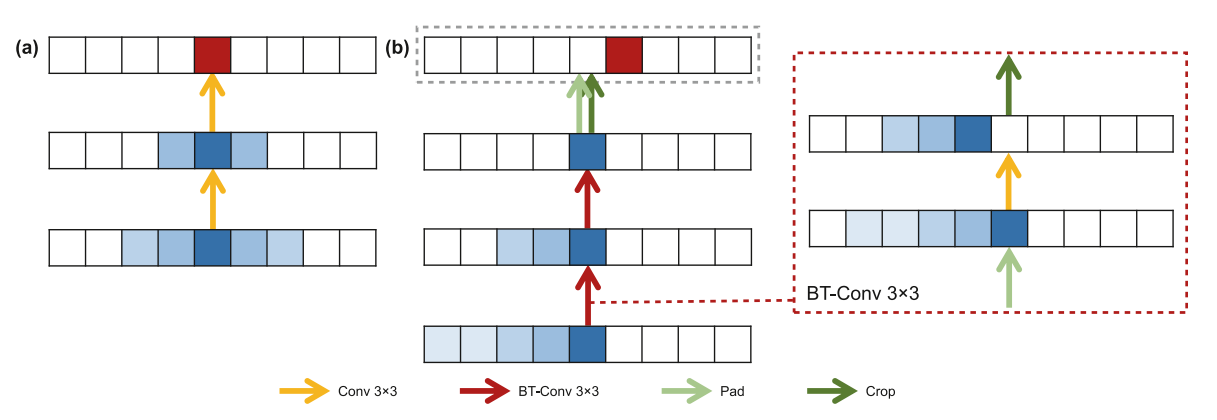


Fig. 4. The convolution operation of (a) the standard U-Net and (b) the BTU-Net.

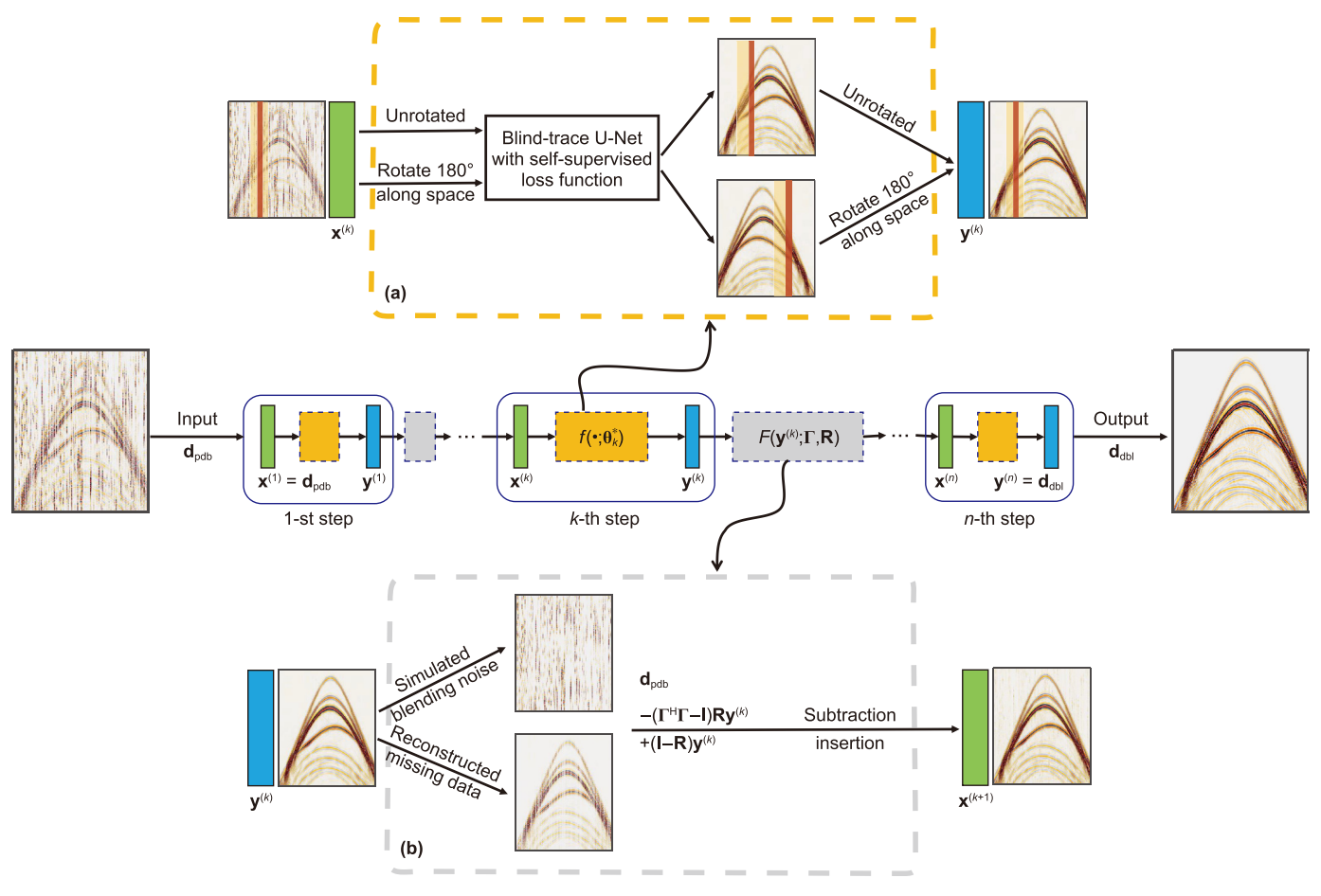


Fig. 5. (a) The single step of self-supervised simultaneous interpolation and deblending using BTU-Net; (b) the process of BNSS and MTRI.

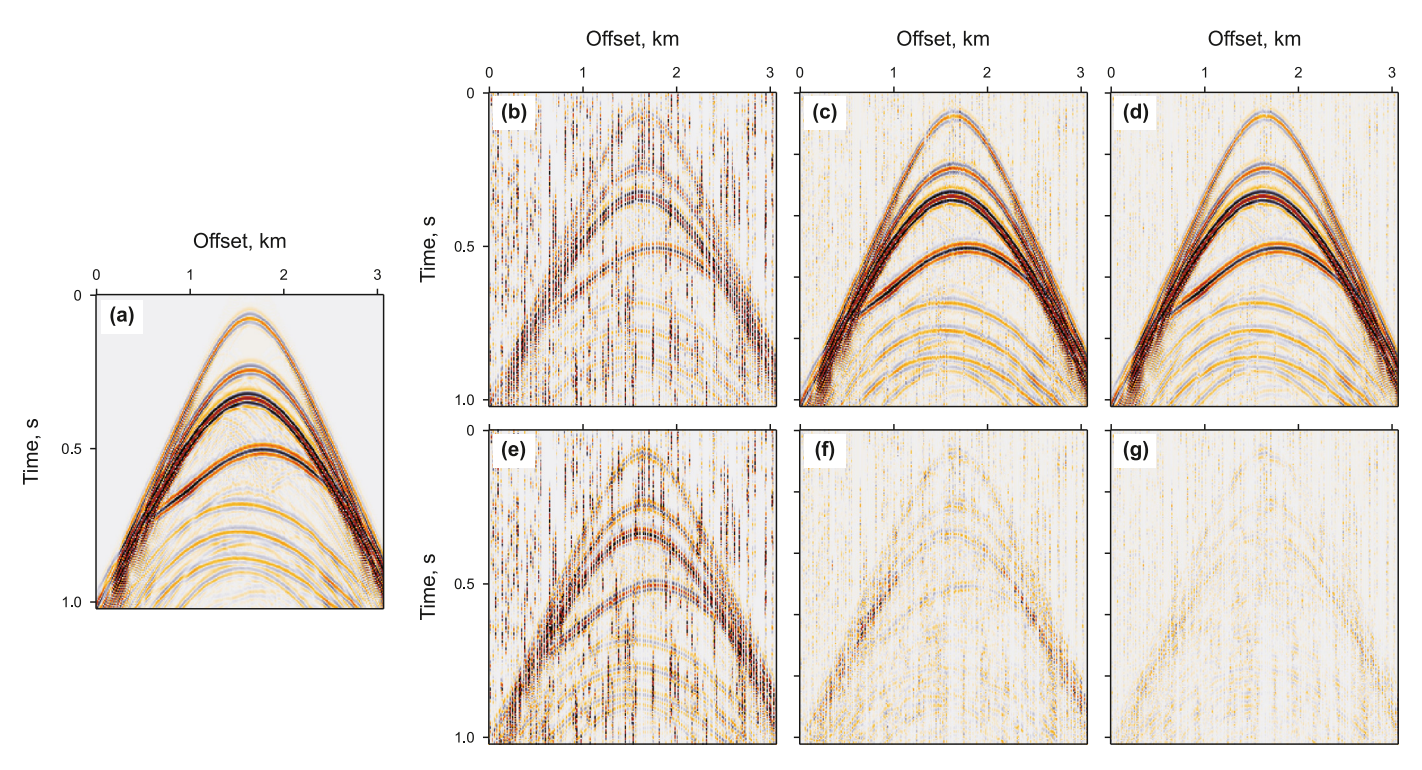


Fig. 6. The input comparisons of each training step. (a) The reference complete unblended data. (b, c, d) The training input of different training steps. (e, f, g) The corresponding difference between (b, c, d) and (a).

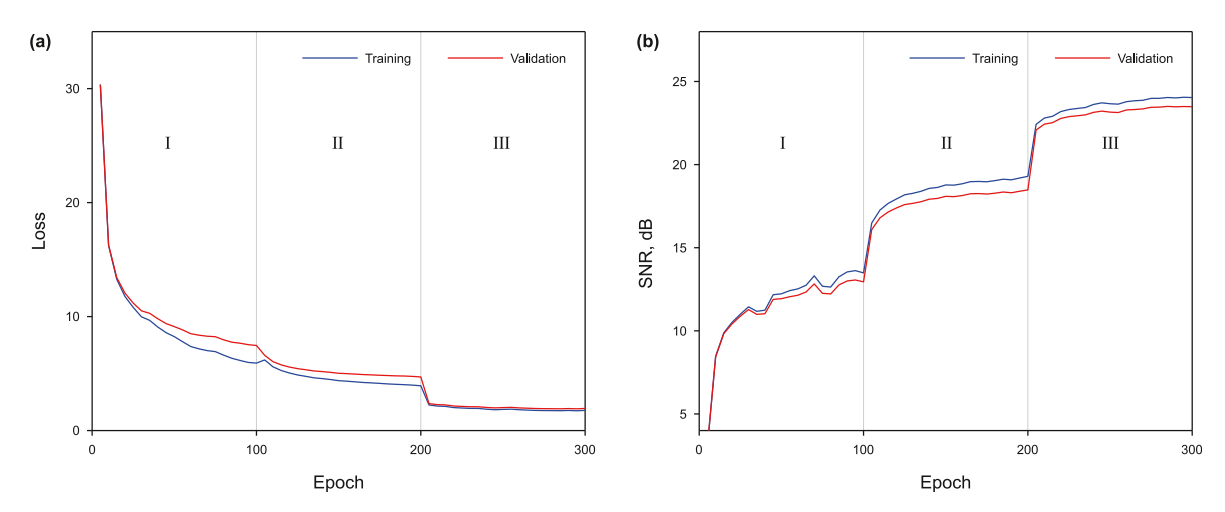


Fig. 7. (a) The loss curve and (b) the recovered SNR curve on training and validation datasets using the three-step self-supervised algorithm for simultaneous deblending and interpolation.

and sampling information is contained in incomplete blended data, we can construct a self-supervised loss function without the need of complete unblended labels,

$$L(\boldsymbol{\theta}) = \left\| \boldsymbol{\Gamma}^{H} \boldsymbol{\Gamma} \boldsymbol{R} f \left(\boldsymbol{d}_{pdb}; \boldsymbol{\theta} \right) - \boldsymbol{d}_{pdb} \right\|_{2}^{2} + \lambda \|\boldsymbol{\Phi}\|_{2}^{2}, \tag{5}$$

where f represents a self-supervised learning network, Φ denotes the convolution kernel with smoothness constrained, and λ is a balance scalar between the smoothness and the L₂ norm measured data misfit. The self-supervised loss function measures the misfit between the simulated incomplete pseudo-deblended result $\Gamma^H \Gamma R f(\mathbf{d}_{pdb}; \theta)$ and the observed one \mathbf{d}_{pdb} . For unblended data, the task simplifies to a pure interpolation issue. Similarly, it changes to a pure deblending issue when there are no missing traces.

Common convolutional networks may encounter the identity mapping problem when being trained with a self-supervised loss function. Blind spot (or blind trace) networks address this issue by incorporating padding and cropping operations before and after the convolutional and max-pooling layers (Laine et al., 2019; Wang et al., 2023b). The BTU-Net, as a modified version of a U-Net, is used to design the network f. The architecture of BTU-Net is depicted in Fig. 3 with red and green arrows highlighting the modifications to the operators. These modifications aim to shift the receptive field leftward, transforming it into a causal filter that relies on left-side traces to predict the target trace.

Specifically, Fig. 4 illustrates the differences in the receptive fields between a standard U-Net convolution (Fig. 4(a)) and the modified version (Fig. 4(b)). The red pixel in each figure represents the same feature location for a clear comparison. The receptive field

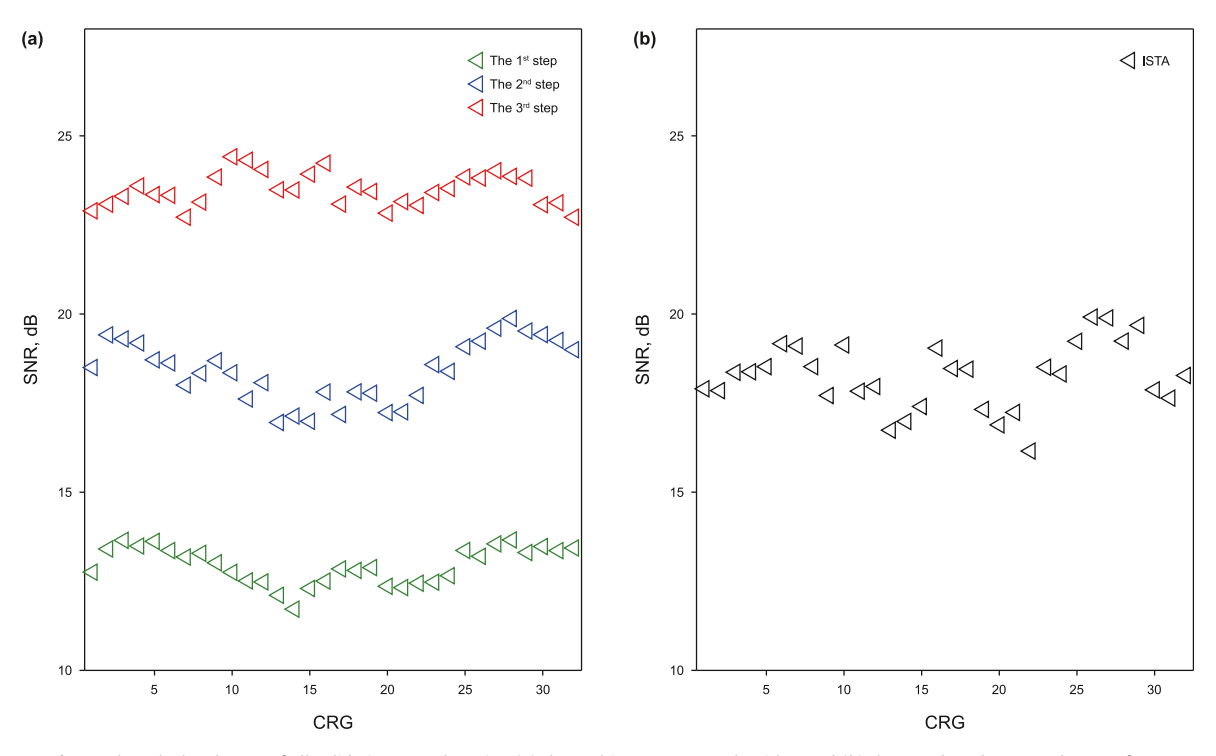


Fig. 8. The calculated SNRs of all validation CRGs by using (a) the multistep BTU-Net algorithm and (b) the ISTA based on curvelet transform.

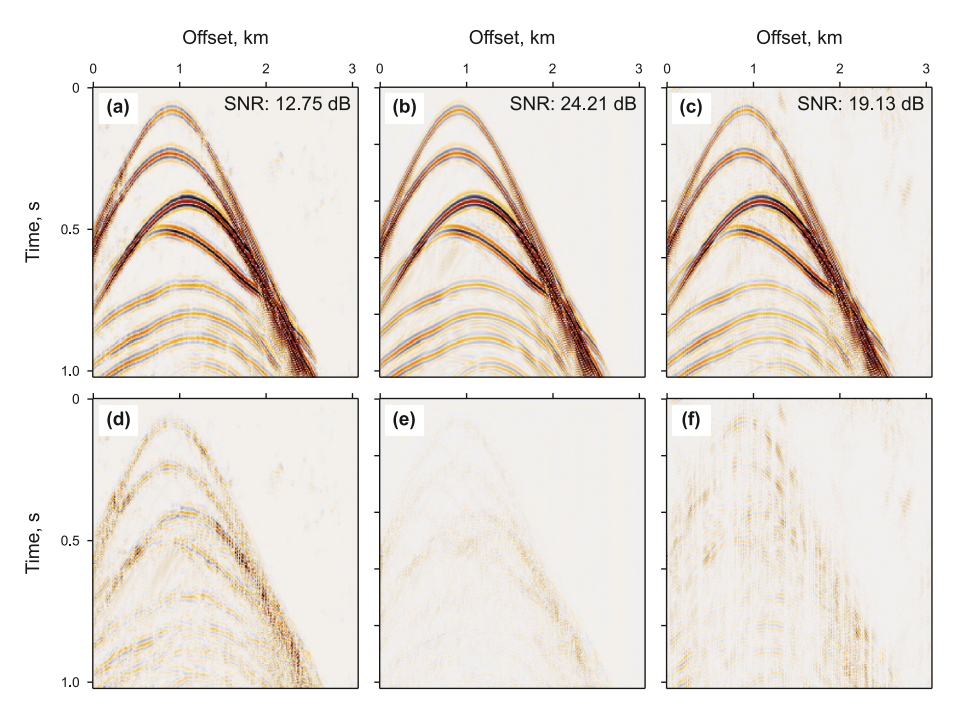


Fig. 9. The recovered results of the 10th validation CRG by using (a) the first step, (b) the sequential first, second, third steps of the multistep BTU-Net algorithm, (c) the ISTA and (d, e, f) the corresponding residuals of (a, b, c).

is marked by the blue pixel, and the shading color indicates the influence of receptive field on the red pixel after convolution operations with a kernel size of 3 \times 3 and a stride of 1. In the standard convolution, the receptive field is symmetrical. The modified convolutional layer of BTU-Net involves padding a null column on the

leftmost side of the input before convolution, and then the rightmost column of the output is cropped, as shown in the red dotted box. To compensate for shifts in the receptive field caused by maxpooling, we also modify the max-pooling with padding and cropping implementations. As a result, the receptive field of the BTU-

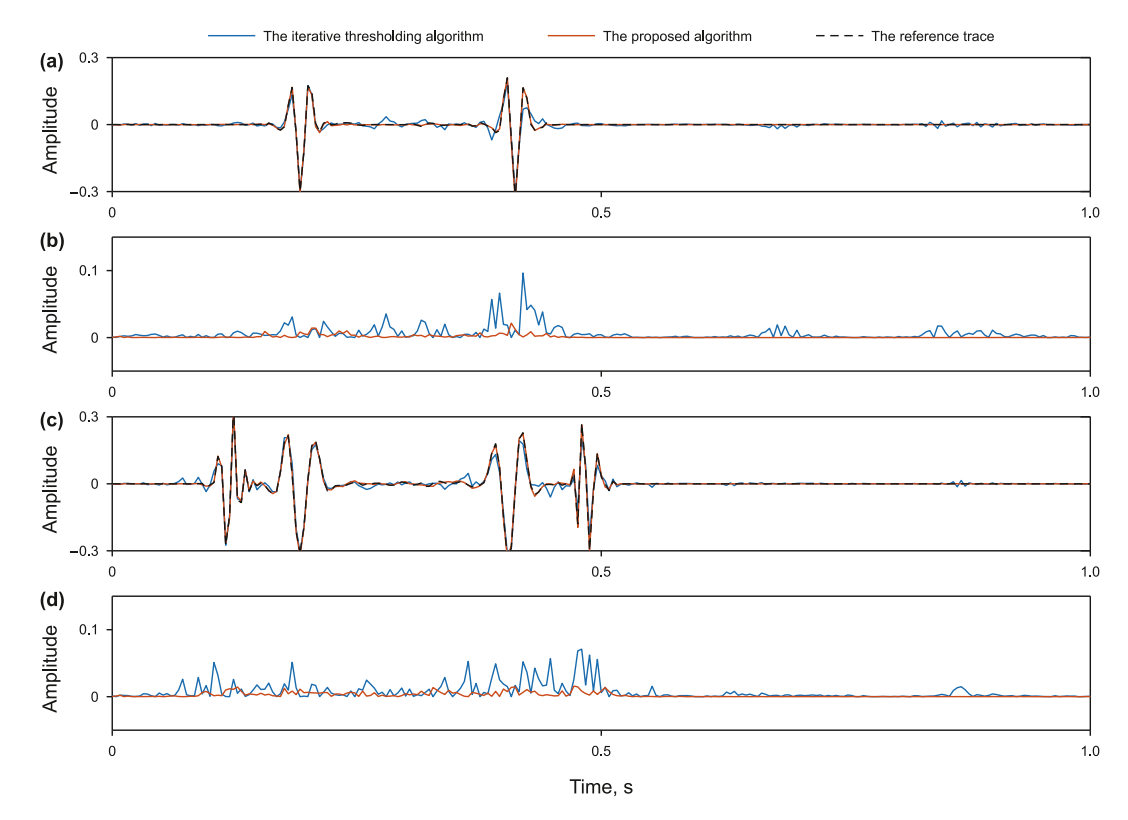


Fig. 10. The single trace comparison of the multistep BTU-Net algorithm and the ISTA. (a) Deblended results and (b) the corresponding residuals of the available 42nd trace; (c) reconstructed results and (d) the corresponding residuals of the unavailable 72nd trace.

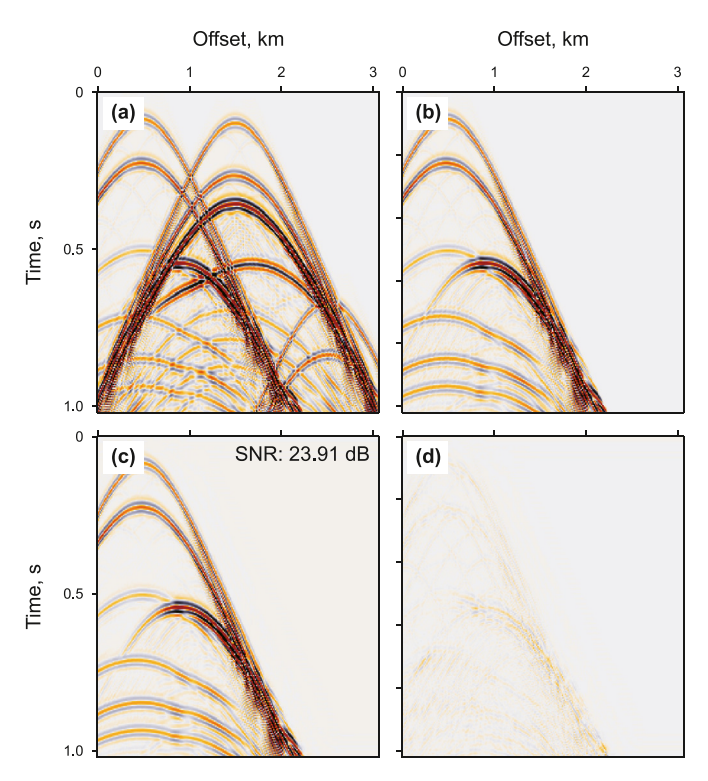


Fig. 11. The 42nd CSG of synthetic dataset. (**a**) Pseudo-deblended CSG; (**b**) unblended CSG; (**c**) deblended CSG of the multistep BTU-Net algorithm; (**d**) the difference between (**c**) and (**b**).

Net shifts leftward compared to that of a standard U-Net. Critically, to prevent learning from identity and to facilitate blind prediction, the leftmost trace is padded and the rightmost trace is cropped in the final output, as shown in the gray dotted box in Fig. 4(b).

BTU-Net predicts the target trace from its left-side traces, functioning as a causal filter. By utilizing the original data (0°) and its spatially flipped version (180°) as inputs, the final predictions can incorporate information from both sides of the target trace, effectively combining causal and anti-causal filtering results (Fig. 5(a)). It should be mentioned that the anti-causal prediction from the spatially 180° flipped data should be flipped back and then arithmetically averaged with the causal prediction from the original data to obtain the current estimation. When the training is convergent, we can obtain the optimized parameters θ_1^* of BTU-Net. While training with both original and spatially 180° flipped data augments the training dataset to ultimately benefit the network training, it also increases the computational load to some extent. Different from pure random noise, blending noise can be iteratively

simulated and subtracted based on the estimated signal. Iterative reconstruction also improves seismic interpolation performance. These strategies can further improve self-supervised deblending and reconstruction performance.

2.4. Multistep self-supervised implementation

The recovered result using BTU-Net with optimized parameters $\boldsymbol{\theta}_1^*$ can be shown as,

$$\mathbf{d}_{\text{dbl}}^{1} = f\left(\mathbf{d}_{\text{pdb}}, \mathbf{\theta}_{1}^{*}\right). \tag{6}$$

However, the obtained results from a single network trained with low-quality input often still contain weak signal leakage and blending noise. The quality of the recovered result is open to improvement. To enhance the recovery performance, a multistep algorithm (Wang et al., 2023) is employed, unfolding as follows.

- 1) Eq. (6) is regarded as the first processing step of simultaneous deblending and interpolation. With the recovered result \mathbf{d}_{dbl}^1 , we can reconstruct missing traces $(\mathbf{I} \mathbf{R})\mathbf{d}_{dbl}^1$ and simulate blending noise $(\Gamma^H \Gamma \mathbf{I})\mathbf{R}\mathbf{d}_{dbl}^1$ based on blending and sampling operators. Then, we subtract the simulated blending noise from incomplete pseudo-deblended data and insert the reconstructed traces to update the input $\mathbf{d}_{pdb} (\Gamma^H \Gamma \mathbf{I})\mathbf{R}\mathbf{d}_{dbl}^1 + (\mathbf{I} \mathbf{R})\mathbf{d}_{dbl}^1$ for the next step, as depicted in Fig. 5(b).
- 2) In the second step, the network is initialized by the optimized parameters $\boldsymbol{\theta}_1^*$ of the first network via transfer learning rather than starting from a randomized initialization. When the network training converges with the loss function $L_2(\boldsymbol{\theta}) = \|\boldsymbol{\Gamma}^H \boldsymbol{\Gamma} \boldsymbol{R} \boldsymbol{f} (\boldsymbol{d}_{pdb} (\boldsymbol{\Gamma}^H \boldsymbol{\Gamma} \mathbf{I}) \boldsymbol{R} \boldsymbol{d}_{dbl}^1 + (\mathbf{I} \mathbf{R}) \boldsymbol{d}_{dbl}^1; \boldsymbol{\theta}) \boldsymbol{d}_{pdb} \|_2^2 + \lambda \|\boldsymbol{\Phi}\|_2^2$, the recovered result is obtained as $\boldsymbol{d}_{dbl}^2 = \boldsymbol{f} (\boldsymbol{d}_{pdb} (\boldsymbol{\Gamma}^H \boldsymbol{\Gamma} \mathbf{I}) \boldsymbol{R} \boldsymbol{d}_{dbl}^1 + (\mathbf{I} \mathbf{R}) \boldsymbol{d}_{dbl}^1; \boldsymbol{\theta}_2^*)$ with the optimized parameters $\boldsymbol{\theta}_2^*$. The blending noise simulation-subtraction (BNSS) and missing traces reconstruction-insertion (MTRI) operations are further used to update the input for the next step.
- 3) A similar procedure is adopted for subsequent processing steps. For the j^{th} step, the training input are updated to $\mathbf{d}_{\text{pdb}} (\mathbf{\Gamma}^{\text{H}} \mathbf{\Gamma} \mathbf{I}) \mathbf{R} \mathbf{d}_{\text{dbl}}^j + (\mathbf{I} \mathbf{R}) \mathbf{d}_{\text{dbl}}^j, j = 2, 3, ..., J$ and the corresponding loss function is updated as $L_{j+1}(\mathbf{\theta}) = \|\mathbf{\Gamma}^{\text{H}} \mathbf{\Gamma} \mathbf{R} f (\mathbf{d}_{\text{pdb}} (\mathbf{\Gamma}^{\text{H}} \mathbf{\Gamma} \mathbf{I}) \mathbf{R} \mathbf{d}_{\text{dbl}}^j + (\mathbf{I} \mathbf{R}) \mathbf{d}_{\text{dbl}}^j; \mathbf{\theta}) \mathbf{d}_{\text{pdb}} \|_2^2 + \lambda \|\mathbf{\Phi}\|_2^2$. The network of the j^{th} step uses the optimized parameters $\mathbf{\theta}_{j-1}^*$ as initialization for training, and we can obtain the

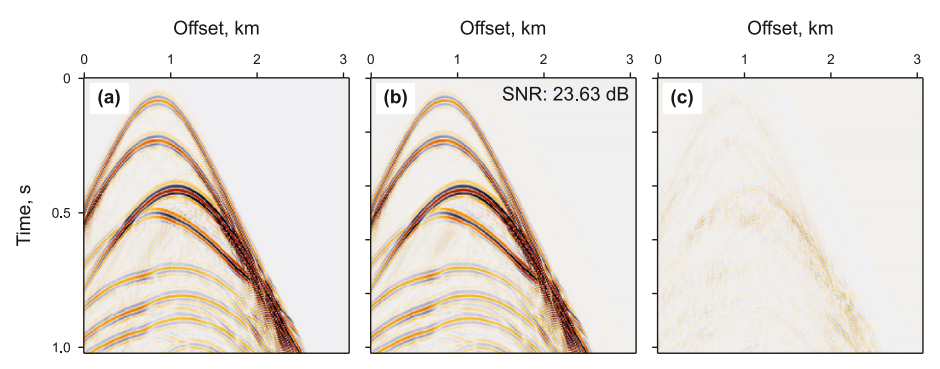


Fig. 12. The 72nd CSG of synthetic dataset. (a) Complete CSG; (b) reconstructed CSG of the multistep BTU-Net algorithm; (c) the residual between (b) and (a).

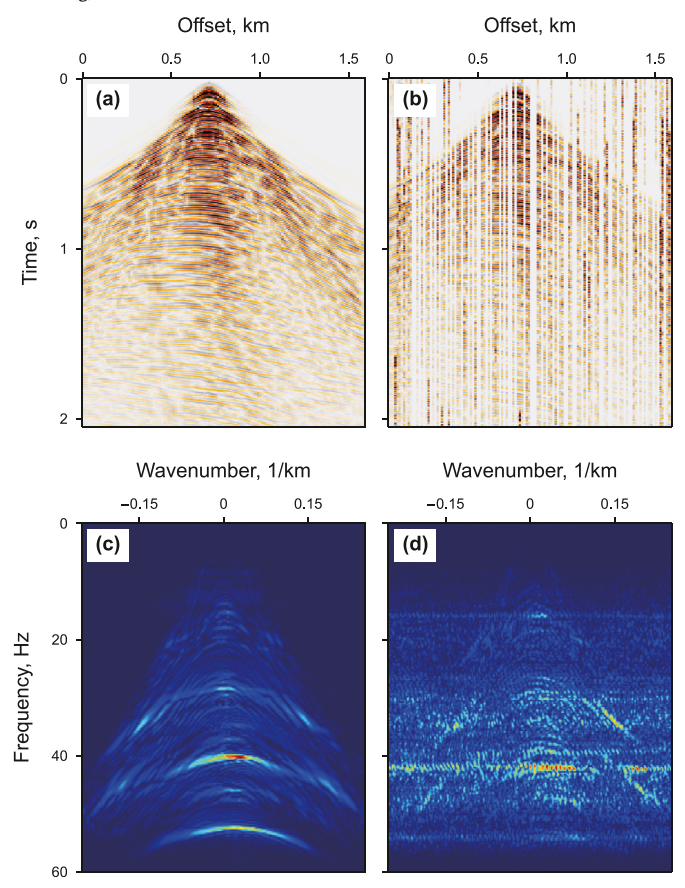


Fig. 13. (a) The reference CRG data; (b) the incomplete pseudo-deblended CRG with a blending fold of 2 and 40% of traces irregularly missing. (c, d) the FK spectra of (a, b).

optimized parameters θ_j^* for subsequent deblending and interpolation to obtain the recovered result \mathbf{d}_{abl}^j .

The multistep algorithm updates the input of the successive network to achieve better prediction at the cost of increased computational burden. The selection of steps and epochs per step should be fine-tuned based on the specific dataset and the convergence status. As the number of steps increases, we tend to

gradually reduce the maximum learning rate, which often results in a corresponding decrease in the epochs per step. We implement three-step deblending after carefully balancing the recovery performance and computational cost. In the future, more efficient training strategy can be researched. The workflow of the multistep BTU-Net based simultaneous deblending and interpolation is depicted in Fig. 5, providing a comprehensive visual representation. The signal-to-noise ratio (SNR) is used to quantitatively evaluate the deblending and reconstruction performance:

$$SNR(dB) = 10 \log_{10} \frac{\|\mathbf{d}\|_{F}^{2}}{\|\mathbf{d} - \mathbf{d}_{dbl}\|_{F}^{2}},$$
 (7)

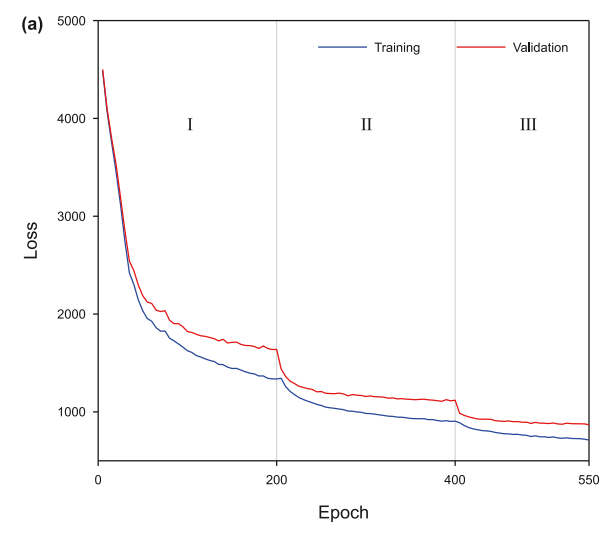
where **d** represents the complete unblended label and \mathbf{d}_{dbl} represents the recovered result, with $\|\cdot\|_F$ denoting the Frobenius norm. Different examples are presented to demonstrate the effectiveness of the newly proposed algorithm in simultaneous deblending and interpolation.

3. Numerical examples

In order to show the validity of the newly proposed method for simultaneous interpolation and deblending, artificially incomplete blended synthetic and field data are used. For detailed comparisons, we present the recovered results of synthetic data using the curvelet-based ISTA.

3.1. Synthetic data example

The data is generated through simulations based on a layered velocity model with a salt body filled with high-velocity. Complete unblended data contains 256 shots, with each shot having 256 uniformly located receivers and 256 sampling points per trace. The spatial interval is 12 m, and the sampling time interval is 4 ms. We artificially sample 50% of the traces in each CRG to emulate missing shots, and then blend them to simulate incomplete blended data with a blending fold of 3. A specific complete unblended CRG is exhibited in Fig. 6(a). After pseudo-deblending, the corresponding incomplete pseudo-deblended result, contaminated by blending noise and irregularities, is exhibited in Fig. 6(b). Using the observed incomplete pseudo-deblended data and its blending and sampling operators, we employ a three-step self-supervised deblending with the details in Fig. 5. The initial input of the network training contains 256 incomplete pseudo-deblended CRGs, which are further



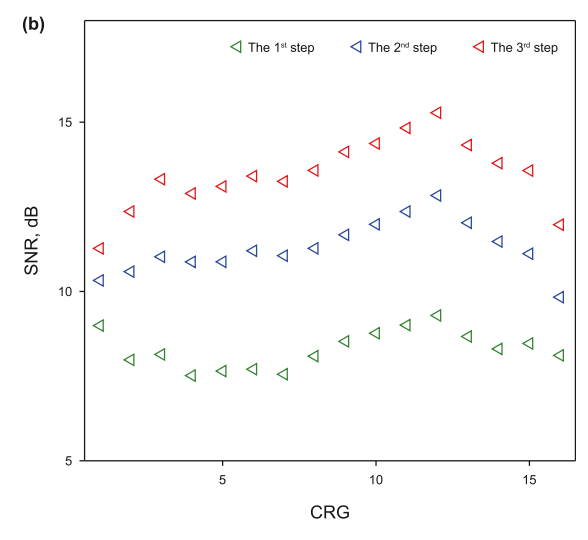


Fig. 14. (a) The loss curves of the training and validation CRGs and (b) the calculated SNRs of all validation CRGs by the multistep BTU-Net algorithm.

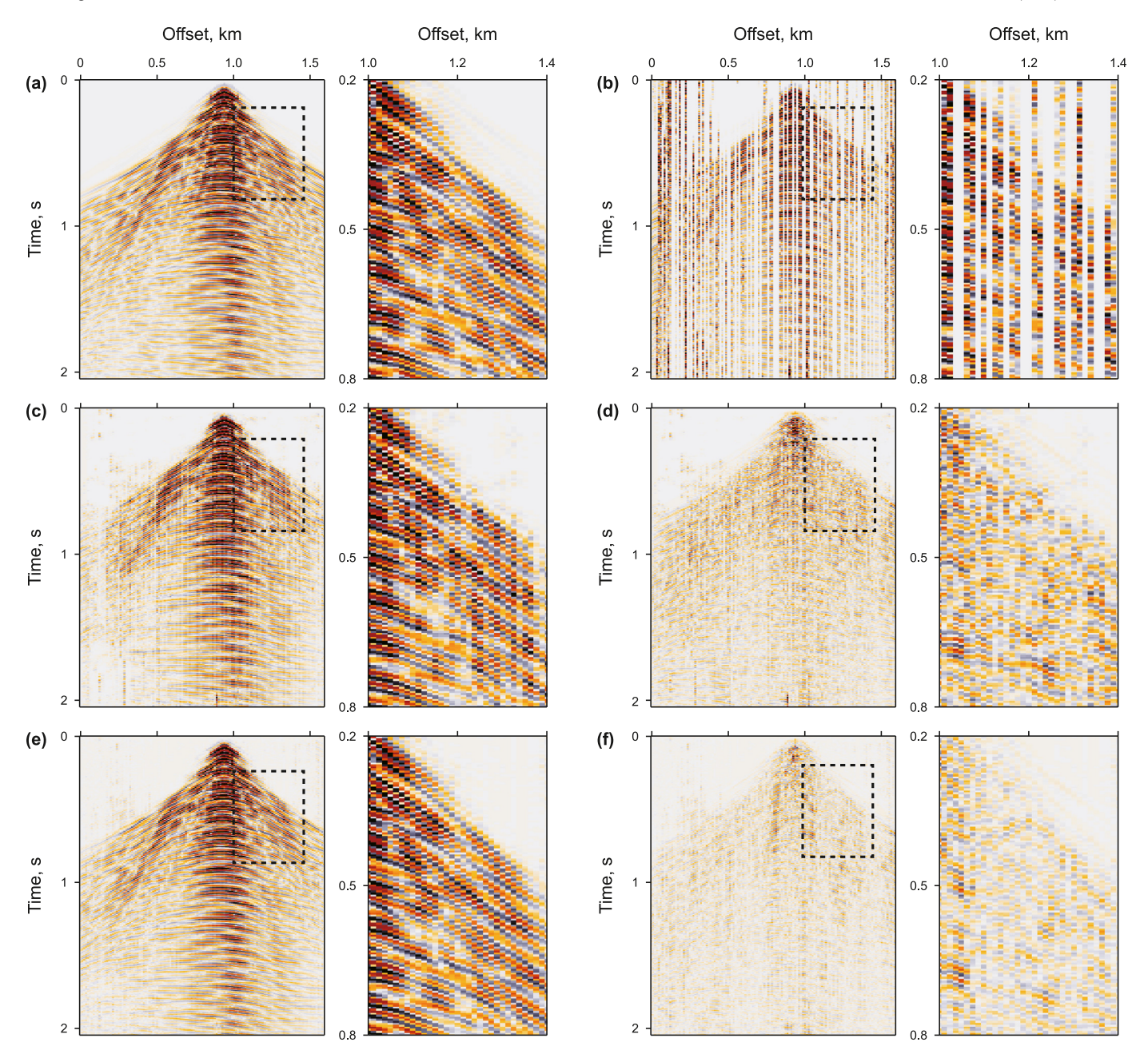


Fig. 15. (a) The reference CRG; (b) the incomplete pseudo-deblended CRG; (c) the recovered result after the first step and (d) the difference between (c) and (a); (e) the sequential first, second, third steps of the multistep BTU-Net algorithm and (f) the difference between (e) and (a).

divided into 224 CRGs for training and 32 CRGs for validation.

After training the current step, we obtain the recovered result, which helps the simulation of blending noise for subtraction from incomplete pseudo-deblended data. Simultaneously, the reconstructed missing traces are inserted to gradually update the input for the subsequent step. To illustrate the decreasing level of blending noise and the increasing interpolation performance of missing traces in the updated input, Fig. 6(c, d) exhibits a specific training input CRG of the second and third steps. The residuals between each input and the reference complete unblended data are also shown in Fig. 6(e, f, g). The comparisons illustrate that the input gradually approaches complete unblended data, with increasing accuracy as the steps progress.

The whole training procedure consists of three steps, with each step containing 100 training epochs. The gradually decreasing loss of the three-step self-supervised algorithm is illustrated in Fig. 7(a). To quantitatively evaluate the deblending and interpolation performance during the network training, we use the complete unblended data as a reference to calculate the recovered SNR, as depicted in Fig. 7(b). It is clear that the optimized multistep self-supervised network is effective, as indicated by the gradual decline and eventual stabilization of the loss in each step, along with the corresponding increase of the recovered SNR.

The 32 validation CRGs are processed by the three-step self-supervised algorithm for simultaneous deblending and interpolation. Fig. 8(a) shows the recovered SNR of all validation CRGs after the first, second, third processing steps. The average SNR after the first step is 12.76 dB, increasing by 5.34 dB in the second step. The final recovered SNR after three sequential deblending steps is 23.52 dB, with an increase of 5.42 dB from the second step.

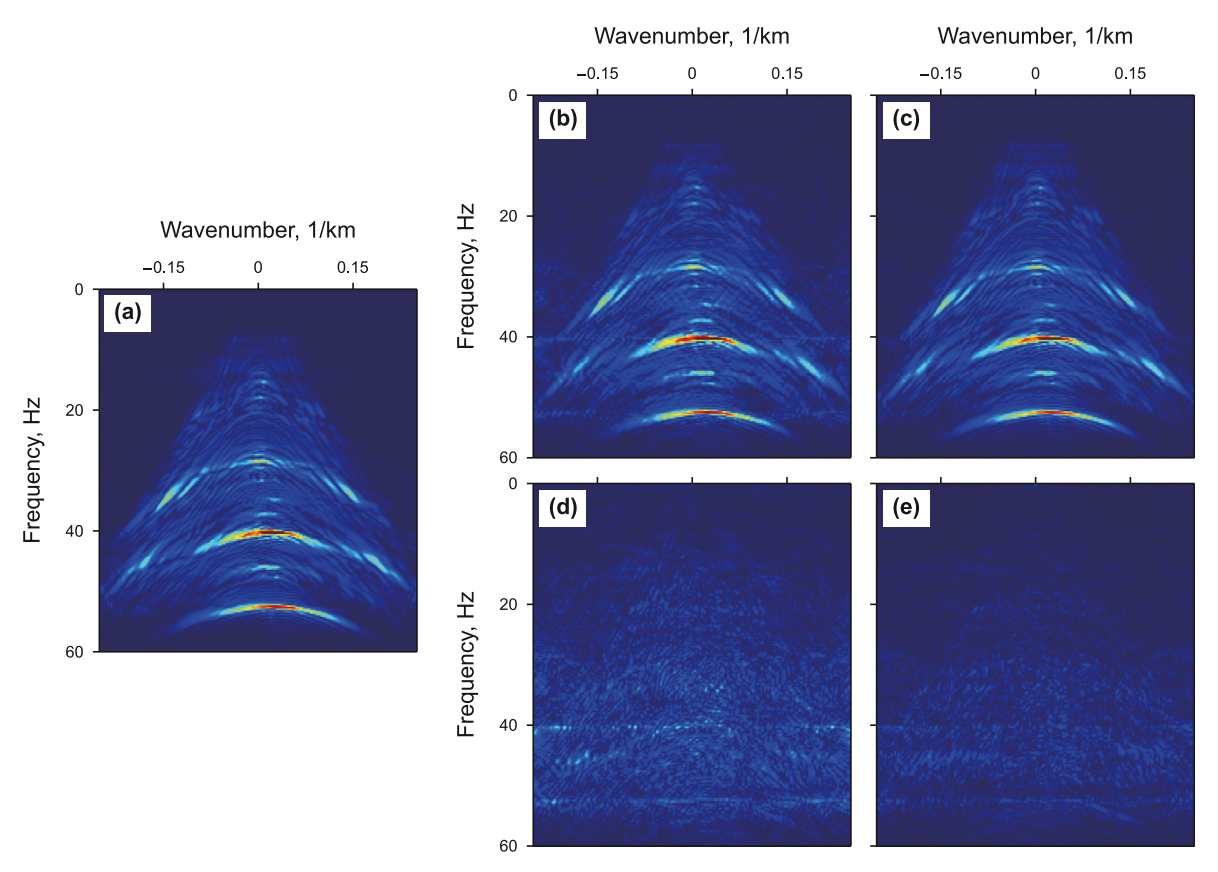


Fig. 16. The comparison of FK spectra of (a) the reference and the recovered results after (b) the first step and (c) the third step. (d, e) The difference between (b, c) and (a).

Comparing the average SNRs across the three steps confirms that the multistep algorithm contributes to a better deblending and interpolation performance. For detailed comparisons, we process all validation CRGs using the curvelet based ISTA with 80 iterations (Wang et al., 2022a) for simultaneous deblending and interpolation, and the recovered SNRs are presented in Fig. 8(b). The multistep BTU-Net algorithm demonstrates superior effectiveness by achieving a higher recovery performance than the ISTA (18.04 dB).

For further analysis, the recovery performance of a specific validation CRG is depicted in Fig. 9. The recovered data from the first processing step is shown in Fig. 9(a) with a recovered SNR of 12.75 dB. A more accurate recovered result via the sequential first, second, and third steps is depicted in Fig. 9(b). Compared to the result in Fig. 9(a), the multistep BTU-Net algorithm significantly enhances recovery performance, achieving a recovered SNR of 24.41 dB. We also depict the recovered result of the ISTA in Fig. 9(c) with a recovered SNR of 19.13 dB for comparisons. The residual between the recovered result and the complete unblended one is depicted in Fig. 9(d, e, f). More residuals exist in Fig. 9(f) compared with Fig. 9(e), which validates the effectiveness of the multistep self-supervised method for high-quality simultaneous deblending and interpolation.

For a specific trace from this validation CRG, the blending noise of an available trace is attenuated and the missing information of an unavailable trace is reconstructed. We extract two traces from Fig. 9 for a detailed single-trace performance analysis. Fig. 10(a) presents the available 42nd trace, demonstrating effective attenuation of the blending noise. Fig. 10(b) illustrates the difference between the deblended result and the reference one. Fig. 10(c) presents the

unavailable 72nd trace, showing that the missing information is reconstructed reasonably. Fig. 10(d) illustrates the difference between the reconstructed result and the reference result. Comparisons in Fig. 10 show that the multistep BTU-Net algorithm outperforms the ISTA in simultaneous deblending and interpolation with significantly less signal leakage.

After processing all incomplete pseudo-deblended CRGs, we can extract all CSGs for performance analysis. Before deblending and interpolation, the unavailable CSGs contain no information, which need to be reconstructed. The available CSGs are contaminated by coherent interference, which need to be attenuated. Fig. 11(a) shows the 42nd CSG, one of the available CSGs, with the unblended data displayed as a reference in Fig. 11(b). Fig. 11(c) and (d) depict the deblended CSG and the residual, respectively, achieving a separation SNR of 23.91 dB. Fig. 12(a) shows the complete version of the 72nd CSG, which, in reality, is unavailable before processing. Fig. 12(b) and (c) depict the reconstructed CSG and the reconstruction residual, respectively, with a reconstruction SNR of 23.63 dB. The effective simultaneous deblending of available CSGs and reconstruction of unavailable CSGs demonstrate the effectiveness of our proposed multistep self-supervised algorithm.

3.2. Field data example

The validity of the multistep self-supervised algorithm is further demonstrated using field data acquired in the Gulf of Suez. The preprocessed field data has 128 shots, each with 128 receivers spaced at every 12.5 m. Per trace has 512 samples with a sampling time interval of 4 ms. Fig. 13(a) illustrates a specific CRG, and incomplete blended field data with a blending fold of 2 and 40% of traces

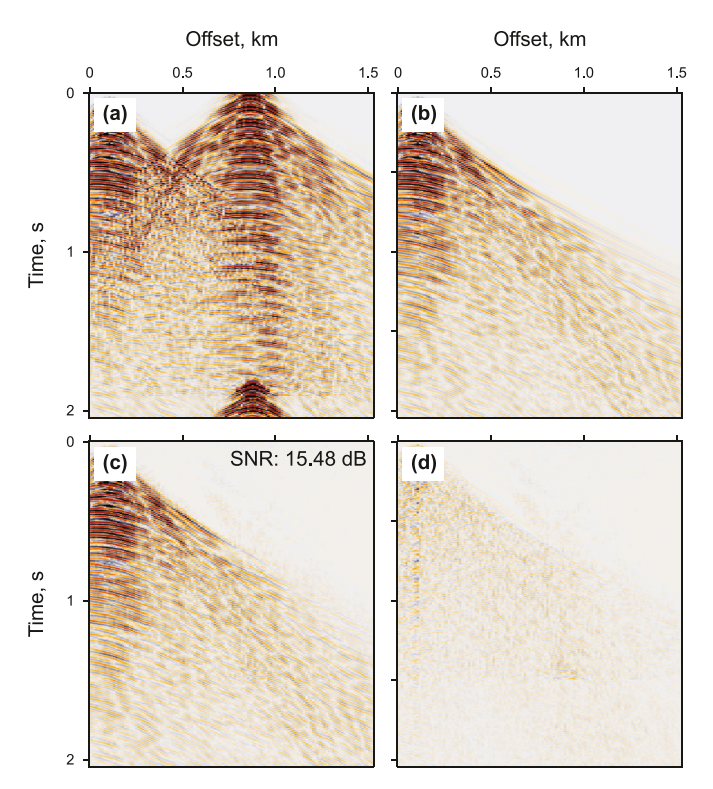


Fig. 17. The 10th CSG of field dataset. (a) Pseudo-deblended CSG; (b) unblended CSG; (c) deblended CSG of the multistep BTU-Net algorithm; (d) the difference between (c) and (b)

irregularly missing is simulated. The corresponding incomplete pseudo-deblended data is displayed in Fig. 13(b). The frequency wavenumber (FK) spectra are depicted in Fig. 13(c) and (d). It shows that the irregularly missing traces and the randomized blending noise manifest as randomized weak-amplitude noise in the FK domain.

Based on the multistep BTU-Net algorithm, 128 incomplete pseudo-deblended CRGs, together with the blending and sampling operators, are fed into the network. During which, 112 CRGs are used for training, and the corresponding rest are used for validation. The training epoch is set to 200, 200, and 150 for the first, second, and third steps. The loss function is provided in Fig. 14(a), and the recovered SNR of the validation CRGs after different training steps is shown in Fig. 14(b).

To visualize the recovery performance of the proposed algorithm, a specific CRG is extracted for a detailed analysis. Fig. 15(a) and (b) illustrate the complete unblended data and the

corresponding incomplete pseudo-deblended data, respectively. Using the proposed self-supervised algorithm, the initial recovered result after the first step is shown in Fig. 15(c). Most of the missing traces are effectively interpolated, and much of the blending noise is attenuated, achieving a recovered SNR of 8.77 dB. However, the signal quality is open to improvement with the recovery residual shown in Fig. 15(d). In order to get high-quality seismic data, the multistep algorithm is applied. Fig. 15(e) depicts the recovered results after the sequential first, second, and third steps and the corresponding residual is depicted in Fig. 15(f) with a recovered SNR of 14.37 dB. To facilitate detailed comparisons, local areas severely affected by missing traces and blending noise, as marked by the dashed box, are enlarged to the corresponding right side. The global and local comparisons show that the proposed multistep self-supervised method effectively improves the recovery accuracy.

For further illustrations, we compare the recovered results in the FK domain, as depicted in Fig. 16. Fig. 16(a) is the FK spectrum of the reference result. Fig. 16(b) and (c) show the deblended and reconstructed results after the first and the third steps of the multistep BTU-Net algorithm, and the residuals are depicted in Fig. 16(d) and (e). Both of the comparisons in the FK domain and the time-space domain verify that the multistep BTU-Net algorithm effectively attenuates the blending noise and reconstructs missing traces as the step progresses.

We also display the recovery performance of CSGs after processing all CRGs. Fig. 17(a) shows a CSG contaminated by coherent blending interference, with the expected unblended CSG displayed in Fig. 17(b) as a reference. Fig. 17(c) shows the deblended result with the coherent blending interference being effectively attenuated, and the separation SNR is of 15.48 dB. The separation residual is shown in Fig. 17 (d). Fig. 18(a) displays another expected complete CSG (unavailable in reality before processing) as a reference. The unavailable CSG is effectively reconstructed using the proposed multistep self-supervised algorithm, as depicted in Fig. 18(b), with a reconstruction SNR of 15.79 dB, and its reconstruction residual is depicted in Fig. 18(c). It shows that the multistep BTU-Net algorithm performs successfully in simultaneous deblending and interpolation.

4. Conclusion

Deep learning algorithms have great potential to nonlinearly characterize seismic data by extracting high-level features for simultaneous seismic deblending and interpolation. Considering the unavailability of complete unblended seismic data, we fully utilize the shooting information during blended acquisition and propose a self-supervised deblending and interpolation algorithm using the BTU-Net. To improve the recovery accuracy, we adopt a multistep strategy with BNSS and MTRI, which improves the input

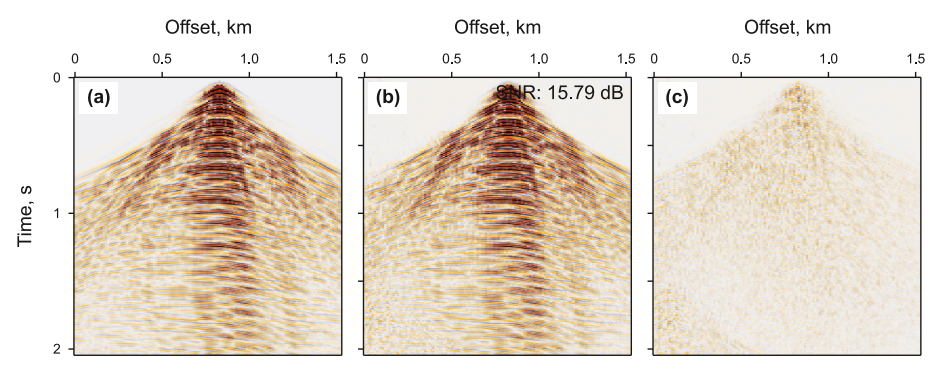


Fig. 18. The 70th CSG of field dataset. (a) Complete CSG; (b) reconstructed CSG of the multistep BTU-Net algorithm; (c) the difference between (b) and (a).

of subsequent steps to achieve high-quality recovered results. The parameters in the current training step are initialized by the optimized parameters in the previous step via transfer learning to improve the training stability and efficiency. The newly proposed algorithm integrates the advantages of the BTU-Net-based self-supervised algorithm and the multistep strategy. Different synthetic and field incomplete blended examples illustrate the effectiveness of the proposed multistep self-supervised BTU-Net algorithm in providing high-quality deblended and interpolated data for subsequent seismic processing.

CRediT authorship contribution statement

Ben-Feng Wang: Writing — review & editing, Writing — original draft, Methodology, Funding acquisition, Formal analysis. **Shi-Cong Lin:** Writing — review & editing, Software. **Xin-Yi Chen:** Writing — review & editing, Validation, Software, Methodology, Investigation.

Conflicts of interests

The authors have no conflicts of interests.

Acknowledgements

This research was financially supported by the National Natural Science Foundation of China (42374134, 42304125, U20B6005), the Science and Technology Commission of Shanghai Municipality (23JC1400502) and the Fundamental Research Funds for the Central Universities.

References

- Abma, R., Howe, D., Foster, M., et al., 2015. Independent simultaneous source acquisition and processing. Geophysics 80, WD37–WD44. https://doi.org/ 10.1190/geo2015-0078.1.
- Abma, R.L., Manning, T., Tanis, M., et al., 2010. High quality separation of simultaneous sources by sparse inversion. 72nd EAGE Conference and Exhibition Incorporating SPE EUROPEC 2010, Cp-161-00019. https://doi.org/10.3997/2214-4609.201400611.
- Akerberg, P., Hampson, G., Rickett, J., et al., 2008. Simultaneous source separation by sparse Radon transform. SEG Technical Program Expanded Abstracts 2008. Society of Exploration Geophysicists SEG Technical Program Expanded Abstracts, pp. 2801–2805. https://doi.org/10.1190/1.3063927.
- Beasley, C.J., Chambers, R.E., Jiang, Z., 1998. A New Look at Simultaneous Sources. SEG Technical Program Expanded Abstracts, pp. 133–135. https://doi.org/10.1190/1.1820149, 1998.
- Berkhout, A.J.G., 2008. Changing the mindset in seismic data acquisition. Lead. Edge 27, 924–938. https://doi.org/10.1190/1.2954035.
- Cao, J., Verschuur, E., Gu, H., et al., 2019. Joint deblending and data reconstruction with focal transformation. Geophysics 84, V219–V231. https://doi.org/10.1190/geo2018-06261
- Chen, X., Wang, B., 2024. Self-supervised multistep seismic data deblending. Surv. Geophys. 45, 383–407. https://doi.org/10.1007/s10712-023-09801-z.
- Chen, Y., 2015. Deblending using a space-varying median filter. Explor. Geophys. 46, 332–341. https://doi.org/10.1071/EG14051.
- Chen, Y., Fomel, S., Hu, J., 2014. Iterative deblending of simultaneous-source seismic data using seislet-domain shaping regularization. Geophysics 79, V179—V189. https://doi.org/10.1190/geo2013-0449.1.
- Chen, Y., Zu, S., Wang, Y., et al., 2020. Deblending of simultaneous source data using a structure-oriented space-varying median filter. Geophys. J. Int. 222, 1805–1823. https://doi.org/10.1093/gii/ggaa189.
- Cheng, J., Sacchi, M.D., 2015. Separation and reconstruction of simultaneous source data via iterative rank reduction. Geophysics 80, V57–V66. https://doi.org/

- 10.1190/geo2014-0385.1.
- Gan, S., Wang, S., Chen, Y., et al., 2016a. Simultaneous-source separation using iterative seislet-frame thresholding. Geosci. Rem. Sens. Lett. IEEE 13, 197–201. https://doi.org/10.1109/LGRS.2015.2505319.
- Gan, S., Wang, S., Chen, Y., et al., 2016b. Separation of simultaneous sources using a structural-oriented median filter in the flattened dimension. Comput. Geosci. 86, 46–54. https://doi.org/10.1016/j.cageo.2015.10.001.
- Huo, S., Luo, Y., Kelamis, P.G., 2012. Simultaneous sources separation via multidirectional vector-median filtering. Geophysics 77, V123–V131. https://doi.org/10.1190/geo2011-0254.1.
- Ibrahim, A., Sacchi, M.D., 2013. Simultaneous source separation using a robust Radon transform. SEG Technical Program Expanded Abstracts 2013. Society of Exploration Geophysicists SEG Technical Program Expanded Abstracts, pp. 4283–4288. https://doi.org/10.1190/segam2013-0447.1.
- Laine, S., Karras, T., Lehtinen, J., et al., 2019. High-quality self-supervised deep image denoising. Adv. Neural Inf. Process. Syst. 32. https://doi.org/10.48550/arXiv.1901.10277
- Luiken, N., Ravasi, M., Birnie, C., 2023. Integrating self-supervised denoising in inversion-based seismic deblending. Geophysics 89, WA39–WA51. https:// doi.org/10.1190/geo2023-0131.1.
- Mahdad, A., Doulgeris, P., Blacquiere, G., 2011. Separation of blended data by iterative estimation and subtraction of blending interference noise. Geophysics 76, O9–O17. https://doi.org/10.1190/1.3556597.
- Richardson, A., Feller, C., 2019. Seismic data denoising and deblending using deep learning. arXiv preprint: 1907.01497. https://doi.org/10.48550/arXiv.1907.01497.
- Sun, J., Hou, S., Vinje, V., et al., 2022. Deep learning-based shot-domain seismic deblending. Geophysics 87, V215–V226. https://doi.org/10.1190/geo2020-0865.1.
- Sun, J., Slang, S., Elboth, T., et al., 2019. A convolutional neural network approach to deblending seismic data. Geophysics 85, WA13—WA26. https://doi.org/10.1190/geo2019-0173.1.
- Wang, B., Han, D., Yuan, C., et al., 2022. Simultaneous interpolation and deblending of 3-D seismic data by iterative thresholding. Geosci. Rem. Sens. Lett. IEEE 19, 1–5. https://doi.org/10.1109/LGRS.2020.3034903.
- Wang, B., Li, J., Luo, J., et al., 2021. Intelligent deblending of seismic data based on U-Net and transfer learning. IEEE Trans. Geosci. Rem. Sens. 59, 8885–8894. https://doi.org/10.1109/TGRS.2020.3048746.
- Wang, B., Chen, X., Li, J., et al., 2023. High dimensional multistep deblending using supervised training and transfer learning. Geophysics 88, WA149—WA159. https://doi.org/10.1190/geo2022-0294.1.
- Wang, K., Hu, T., 2022. Deblending of seismic data based on neural network trained in the CSG. IEEE Trans. Geosci. Rem. Sens. 60, 1–12. https://doi.org/10.1109/ TGRS.2021.3121806.
- Wang, K., Hu, T., Wang, S., 2023a. Iterative deblending using unsupervised learning with double-deep neural networks. Geophysics 88, V187–V205. https://doi.org/ 10.1190/geo2022-0299.1.
- Wang, S., Hu, W., Yuan, P., et al., 2023b. A self-supervised deep learning method for seismic data deblending using a blind-trace network. IEEE Transact. Neural Networks Learn. Syst. 34, 3405–3414. https://doi.org/10.1109/
- Xu, W., Zhou, Y., Liu, D., et al., 2021. Seismic simultaneous source separation via an unsupervised deep learning method. 82nd EAGE Annual Conference & Exhibition 1–5. https://doi.org/10.3997/2214-4609.202112628, 2021.
- Xu, W., Lipari, V., Bestagini, P., et al., 2022. Intelligent seismic deblending through deep preconditioner. Geosci. Rem. Sens. Lett. IEEE 19, 1–5. https://doi.org/ 10.1109/lgrs.2022.3193716.
- Xue, Y., Chen, Y., Jiang, M., et al., 2022. Unsupervised seismic data deblending based on the convolutional autoencoder regularization. Acta Geophys. 70, 1171–1182. https://doi.org/10.1007/s11600-022-00772-0.
- Zhou, Y., Li, S., 2018. Simultaneous deblending and interpolation using structure-oriented filters. J. Appl. Geophys. 150, 230–243. https://doi.org/10.1016/j.jappgeo.2018.01.015.
- Zu, S., Cao, J., Qu, S., et al., 2020. Iterative deblending for simultaneous source data using the deep neural network. Geophysics 85, V131–V141. https://doi.org/ 10.1190/geo2019-0319.1.
- Zu, S., Ke, C., Hou, C., et al., 2022. End-to-end deblending of simultaneous source data using Transformer. Geosci. Rem. Sens. Lett. IEEE 19, 1–5. https://doi.org/ 10.1109/LGRS.2022.3174106.
- Zu, S., Zhou, H., Chen, Y., et al., 2016. A periodically varying code for improving deblending of simultaneous sources in marine acquisition. Geophysics 81, V213–V225. https://doi.org/10.1190/geo2015-0447.1.